Secondary-structure characterization by far-UV CD of highly purified uncoupling protein 1 expressed in yeast

Pierre DOUETTE*, Rachel NAVET*, Fabrice BOUILLENNE†, Alain BRANS†, Claudine SLUSE-GOFFART*, André MATAGNE† and Francis E. SLUSE*[1]

*Laboratory of Bioenergetics, Centre for Oxygen Research and Development, Institute of Chemistry B6, University of Liege, Sart Tilman, B-4000 Liege, Belgium, and †Centre for Protein Engineering, Institute of Chemistry B6, University of Liege, Sart Tilman, B-4000 Liege, Belgium

The rat UCP1 (uncoupling protein 1) is a mitochondrial inner-membrane carrier involved in energy dissipation and heat production. We expressed UCP1 carrying a His_6 epitope at its C-terminus in *Saccharomyces cerevisiae* mitochondria. The recombinant-tagged UCP1 was purified by immobilized metal-ion affinity chromatography to homogeneity (>95 %). This made it suitable for subsequent biophysical characterization. Fluorescence resonance energy transfer experiments showed that n-dodecyl-β-D-maltoside-solubilized UCP1–His_6 retained its PN (purine nucleotide)-binding capacity. The far-UV CD spectrum of the functional protein clearly indicated the predominance of α-helices in the UCP1 secondary structure. The UCP1 secondary structure exhibited an α-helical degree of approx. 68 %, which is at least 25 % higher than the previously reported estimations based on computational predictions. Moreover, the helical content remained unchanged in free and PN-loaded UCP1. A homology model of the first repeat of UCP1, built on the basis of X-ray-solved close parent, the ADP/ATP carrier, strengthened the CD experimental results. Our experimental and computational results indicate that (i) α-helices are the major component of UCP1 secondary structure; (ii) PN-binding mechanism does not involve significant secondary-structure rearrangement; and (iii) UCP1 shares similar secondary-structure characteristics with the ADP/ATP carrier, at least for the first repeat.

Key words: CD, fluorescence resonance energy transfer, homology modelling, mitochondrial membrane protein, secondary structure, uncoupling protein.

INTRODUCTION

UCP1 (uncoupling protein 1) is a mitochondrial inner-membrane protein found in thermogenic brown adipocytes and belongs to the large MCF (mitochondrial carrier family) [1]. It dissipates energy into heat by catalysing the re-entry of protons of the electrochemical gradient built up by the respiratory chain (see [2] for a review). Its function is activated by NEFA (non-esterified fatty acid) and is inhibited by PNs (purine nucleotides). Moreover, its activity seems to depend on the presence of coenzyme Q, a redox intermediate of the respiratory chain. The latter may act as an obligatory cofactor for UCP1 activity [3]. However, the mechanism of the NEFA-mediated proton import and its regulation need to be elucidated at the molecular level.

To date, very little structural information is available for the UCP1 as well as for other UCP subfamily members. This is mainly due to the difficulty in obtaining large amounts of native, i.e. functional, protein purified to homogeneity. Similar to the other members of the MCF, the nuclear-encoded *UCP1* gene exhibits a triplicated structure leading to a 3-fold repeat of approx. 100 amino acids. According to the sequence alignments and the hydrophobicity profiles, it has been hypothesized that these three domains have related sequences yielding similar secondary structures. A widely accepted model proposed by Runswick et al. [4] has finally emerged from computational analyses of UCP1, AAC (ADP/ATP carrier) and phosphate carrier sequences and has been further extended to all members of the MCF. This model suggests that six membrane-spanning α-helices, two in each domain, are connected by large loop protrusions of undefined secondary structure that are consecutively located at the matrix and cytosol sides [5]. This topological model has been strengthened by the study of antigenic sites conducted on UCP1 by Miroux et al. [6]. On the basis of hydrophobicity profiles and considering a minimized number of polar residues in helix segments due to energy constraints, membrane-spanning helices were defined with an average length of 19 and 21 residues respectively within odd- and even-numbered helices [7,8]. Thus approx. 120 residues are suspected to adopt a helical conformation; hence a helical degree of approx. 40 % can be deduced.

Recently, the X-ray structure of the mitochondrial AAC1, a member of the MCF, has been obtained at 2.2 Å (1 Å = 0.1 nm) resolution in the carboxyatractyloside-inhibited conformation [9]. When AAC1 secondary-structure contents calculated from X-ray crystallography and from computational predictions are compared, numerous structural differences can be pointed out. Indeed, lengths of odd- and even-numbered helices as well as the presence of small hydrophilic helices within the three-matricial loops have been badly predicted from hydropathy profiles of the primary structure. Both transmembrane domains and hydrophilic helices actually increase the helical content to 66 % (195/297 amino acids), which is at least 25 % more than the previous predicted model.

In contrast with other eukaryotic cells, no homologue of UCP1 is found in yeast *Saccharomyces cerevisiae* mitochondria. Therefore recombinant UCP expressions have been previously achieved in *S. cerevisiae* [10]. After the induction of the phosphoglycerate kinase promoter-controlled expression (pKV49 vector), strong expression has led to a marked growth defect of the yeast [11] and, at the highest expression level, to a mitochondrial 'uncoupling artifact', i.e. a PN-insensitive NEFA-stimulated

Abbreviations used: AAC, ADP/ATP carrier; DDM, n-dodecyl β-D-maltoside; FRET, fluorescence resonance energy transfer; HTP, hydroxyapatite; IMAC, immobilized metal-ion affinity chromatography; LA, linoleic acid; Mant, *N*-methylanthraniloyl; MCF, mitochondrial carrier family; NEFA, non-esterified fatty acid; Ni-NTA, Ni^{2+}-nitrilotriacetate; PN, purine nucleotide; RMSD, root mean square deviation; SVD, singular-value decomposition; TX100, Triton X-100; UCP, uncoupling protein.

[1] To whom correspondence should be addressed (e-mail F.Sluse@ulg.ac.be).

proton leak. This phenomenon has been putatively linked to the rate of UCP1 synthesis [12].

In the present study, a yeast-based expression system has been used to produce and purify sufficient quantities of UCP1 for subsequent biophysical characterization. Furthermore, we report a new expression and purification strategy that leads to a homogeneous and functional UCP1. Thus we have expressed UCP1 carrying a His_6 epitope at its C-terminus in the yeast *S. cerevisiae*, at a mild level that does not lead to an artifactual uncoupling described with the pKV49 vector. After detergent solubilization, purification of the yeast-expressed UCP1–His_6 was performed to homogeneity by a two-step strategy including an HTP (hydroxyapatite) step followed by IMAC (immobilized metal-ion affinity chromatography). We probed the GTP-binding capacity of the detergent-solubilized purified protein by FRET (fluorescence resonance energy transfer). The secondary-structure content of both GTP-free and GTP-inhibited UCP1 has been determined by far-UV CD analysis. Analysis of these results clearly demonstrates that high helical content is the major structural feature of UCP1, which is not modified by PN binding.

EXPERIMENTAL

Chemicals

DDM (n-dodecyl β-D-maltoside) Anagrade was purchased from Anatrace (Maumee, OH, U.S.A.), membrane protein grade TX100 (Triton X-100) was from Roche and Mant (*N*-methyl-anthraniloyl)-ATP was from Molecular Probes. BSA, ATP and GTP were purchased from ICN Biomedicals (Asse-Relegem, Belgium). CHT Ceramic HTP type II was purchased from Bio-Rad Laboratories and Ni-NTA (Ni^{2+}-nitrilotriacetate) resin was from Novagen. Devices for dialysis were purchased from Pierce (Slide-A-Lyzer Dialysis cassette, 10 000 Da molecular mass cut-off). All other reagents were of the highest purity grade.

Protein expression in *S. cerevisiae*

After PCR amplification, rat *UCP1* gene (kindly provided by Dr F. Bouillaud, Centre National de la Recherche Scientifique, Meudon, France) was inserted into pYES 2.1/Topo TA cloning vector (Invitrogen) containing the *URA3* gene for selection and *GAL1* promoter and enhancer for a galactose-inducible expression. The forward primer (5′-AACAAAATGGTGAGTT-CGACAACTTCC-3′) contained a Kozak sequence (underlined) at the translation initiation site to increase the translation of the protein [13]; the reverse primer [5′-CTA-$(ATG)_6$-TGTGGTGC-AGTCCACTGT-3′] contained the sequence coding for the His_6 tag (underlined) to allow the affinity purification of UCP1–His_6 on IMAC. After verifying the sequence of the insert (ALF Express, Amersham Biosciences), the plasmid was transformed into *Escherichia coli* Top10F′ strain, purified and subcloned into *S. cerevisiae* diploid INVSc1 (a/α) strain (Invitrogen).

Cultures were grown in either 2 litre flasks or 15 litre fermenter (BioFlow 4500; New Brunswick Scientific, Rotselaar, Belgium) after 48 h precultures (100 ml and 1 litre respectively). Expression was induced for 4–16 h. The preculture was conducted in SC (*S. cerevisiae*) minimal medium containing 0.67 % (w/v) yeast nitrogen base, 0.25 % (w/v) $(NH_4)_2SO_4$, 0.01 or 0.05 % (w/v) amino acids and 2 % (w/v) glucose. Glucose repressed *GAL1*-promoted gene expression. Induction medium was the one used for preculture, except for the carbon source that was 2 % (w/v) galactose.

Cells were harvested from 15 litre fermenters with a D_{600} of approx. 8.0. Mitochondria were isolated after the generation of spheroplasts by zymolyase 20T (ICN Biomedicals), as described by Daum et al. [14]. During NEFA-depleting steps, BSA concentration varied from 0.1 to 1 % (w/v) from one flask preparation to another. BSA was removed by two washing steps in 20 mM Tris and 0.65 M mannitol (pH 7.5), and mitochondria were resuspended into the same buffer at a final concentration of 50 mg/ml. Mitochondrial respiration (1 mg of mitochondrial protein) was assayed at 25 °C using a Clarck-type electrode (Hansatech, King's Lynn, Norfolk, U.K.) in respiration buffer (10 mM Tris/0.65 M mannitol/0.5 mM EGTA/ 2 mM $MgCl_2$/10 mM KH_2PO_4, pH 6.9) containing 2 mM NADH and 1 mM succinate. Mitochondrial UCP1–His_6 content was evaluated by Western blotting (using anti-His-tagged antibodies) with purified UCP1–His_6 as a standard.

Protein purification

Typically, 50 mg of mitochondrial proteins was solubilized at a final concentration of 10 mg/ml in 20 mM Tris, 20 mM Na_2SO_4, 0.25 mM EDTA, protease inhibitor cocktail (pH 6.8) supplemented with 1–2 % (w/v) TX100. After 1 h of incubation at 4 °C, the mitochondrial sample was centrifuged at 20 000 ***g*** for 20 min at 4 °C. The supernatant was then applied on HTP resin at a flow rate of 2 ml/min using an Åkta Station (Amersham Biosciences; 10 mg of total protein/ml of settled gel, equilibrated with 5 mM Tris, 20 mM Na_2SO_4, 0.25 mM EDTA and 0.05 % TX100). UCP1–His_6 and also two major contaminants did not bind the resin and were recovered in the flow-through fraction. HTP fraction was supplemented with 50 mM NaH_2PO_4/Na_2HPO_4, 100 mM NaCl and 1 mM $MgCl_2$, and applied on Ni-NTA resin (Novagen) equilibrated in 50 mM NaH_2PO_4/Na_2HPO_4, 100 mM NaCl and 0.05 % TX100. The final protein amount/resin volume ratio was set to 1. The batch incubation was performed for 2 h at 4 °C under stirring. The resin was mounted on to a small column and washed with 100 resin vol. of washing buffer containing 20 mM Tris, 100 mM NaCl, 20 mM imidazole and 0.02–0.05 % of detergent (TX100 or DDM; see the Results and Discussion section). The protein was finally eluted at a final concentration of 0.2–0.4 mg/ml in washing buffer supplemented with 500 mM imidazole. Imidazole was removed by extensive dialysis. Protein concentration was determined with *DC* Protein assay kit (Bio-Rad Laboratories).

SDS/PAGE and Western blotting

Proteins were subjected to electrophoresis in 8 or 10 % SDS/polyacrylamide gel and analysed by Coomassie Blue staining or Western blotting. Western blotting was performed with a Trans-blot semi-dry transfer cell (Bio-Rad Laboratories). Proteins were transferred to PVDF membrane (Immobilon-P; Millipore) and revealed by using BM Chemiluminescence Western blotting kit (Roche). Briefly, the membrane was blocked for 1 h at room temperature (20 °C) in blocking buffer [50 mM Tris/100 mM NaCl, pH 7.5/1 % (v/v) blocking reagent], incubated for 1 h at room temperature with anti-His_6 antibody coupled with peroxidase (Roche), washed three times in 50 mM Tris, 100 mM NaCl (pH 7.5), 0.1 % (v/v) Tween 20 and finally exposed for 10 s to 1 min to Hyperfilm ECL® (Amersham Biosciences). Protein content estimations on Coomassie Blue-stained gels and autoradiographed films were performed with NIH ImageJ software.

FRET and nucleotide-binding measurement

The PN-binding capacity of isolated UCP1–His_6 was assayed by FRET in a PerkinElmer LS50B spectrofluorimeter. Excitation

and emission wavelengths were 280 and 435 nm respectively with slit widths of 3 and 5 nm respectively and the scan speed was 100 nm/min. FRET experiments were performed in 100 μl microcuvettes (Hellma, Müllheim, Germany), with a path length of 0.3 cm. Fluorescence of 10 μM Mant-ATP was measured at room temperature in the presence of 150 μg/ml purified UCP1 (approx. 5 μM). The buffer contained 10 mM Tris, 100 mM NaCl (pH 6.8) and 0.05 % DDM. Binding equilibrium was displaced by adding 1 mM unmodified ATP. For each sample, five spectra were collected, averaged and baseline-corrected by subtraction of blank buffer.

CD measurements

Before CD analysis, DDM-solubilized purified UCP1–His_6 was extensively dialysed (three times, 100 vol. of sample) against 5 mM Tris and 0.03 % DDM (pH 6.8).

CD measurements were made in a Jasco J-810 spectropolarimeter, in the amide band (190–240 nm) at a protein concentration of 150 μg/ml (approx. 5 μM). Spectra were acquired in a 0.1 cm cell path length at a scan speed of 20 nm/min, with a 1 nm bandwidth and a 4 ms response. The spectra were measured 10-fold, averaged and baseline-corrected by subtraction of blank buffer. For measurements, performed in the presence of GTP, a high-GTP concentration stock (100 mM) was used to avoid protein dilution and the mixture was left to equilibrate for 5 min before CD recording.

The far-UV CD spectra were analysed on DichroWeb website [15,16], using CDSSTR [17,18] and SELCON3 [19,20] algorithms, with the basis set including CD spectra of 43 globular proteins of solved structure [21]. The SVD (singular-value decomposition) algorithm assigned native and GTP-inhibited UCP1 secondary structures.

Homology modelling

Sequence alignments of rat UCP1 and bovine heart AAC1 (SwissProt accession nos P04633 and P0272 respectively) were performed with ClustalW. The length of UCP1 repeats was determined either by internal alignment of UCP1 repeats or by UCP1/AAC1 alignment. The automated comparative modelling server Swiss-Model located at ExPASY was employed to generate a model of UCP1 repeat 1 with AAC1 structure as the template (PDB accession no. 1OKC). The model reliability was determined on the basis of Cα RMSD (root mean square deviation). RMSD values were calculated with Swiss-PDB Viewer [22]. PROCHECK [23] was used to calculate the secondary structure from PDB files.

RESULTS AND DISCUSSION

Expression of UCP1–His_6 in yeast mitochondria

To enable purification of UCP1 to homogeneity, we exploited IMAC approach after introducing six histidine residues at the C-terminus of the protein. The addition of the C-terminal epitope was achieved by PCR amplification as well as a Kozak sequence. Since we were looking for a mild expression to avoid artifactual uncoupling due to high-level expression of recombinant UCP1 in yeast [12], *GAL1* promoter, inducible on galactose addition, was used. The yeast-expressed UCP1–His_6 exhibited an expected 36 kDa band, which was revealed by Coomassie Blue (Figure 1A). After overnight induction with 2 % galactose at 28 °C, total mitochondrial proteins were analysed by Western blotting with antibodies directed against the His epitope. In these expression conditions, expression level was evaluated to approx. 10 μg/mg of total mitochondrial proteins. Moreover, this expression level did not induce a strong growth defect of the culture but only a slow down of 15–20 % (results not shown).

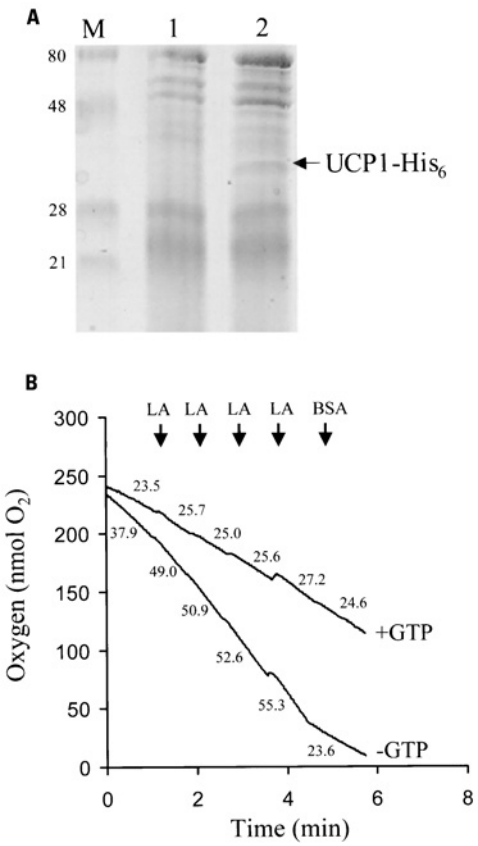

Figure 1 Analysis of UCP1–His_6 expression in yeast mitochondria and LA-stimulated GTP-sensitive uncoupling activity on isolated mitochondria

(**A**) Total mitochondrial proteins (50 μg/lane) from isolated mitochondria were subjected to SDS/PAGE (12 % gel) and analysed by Coomassie Blue staining. Yeast mitochondria were isolated from non-induced culture (lane 1) or from culture induced with 2 % galactose for 16 h at 28 °C (lane 2). A marked band (arrow) appeared at approx. 36 kDa corresponding to UCP1–His_6. M, molecular-mass standards (kDa). (**B**) Mitochondria (1 mg) were incubated at 25 °C with a respiration buffer containing 2 mM NADH and 1 mM succinate in the absence or presence of GTP as mentioned. Successive additions of LA (final concentrations of 1, 2, 5 and 10 μM, downward-pointing arrows) led to an increase in respiration rate in the absence of GTP. NEFA removal was achieved by a final addition of 0.1 % BSA (downward-pointing arrow). Numbers on the traces refer to respiration rates in nmol of oxygen · min^{-1} · (mg of protein)$^{-1}$.

After 16 h of induction with 2 % galactose, the isolated mitochondria showed an NEFA-activated PN-sensitive uncoupling activity. Indeed, increasing concentrations of LA (linoleic acid) stimulated non-phosphorylating respiration, and the presence of an UCP1 inhibitor, such as GTP, cancelled this LA-sustained respiration (Figure 1B). The non-phosphorylating respiration was stimulated 2.5-fold by 10 μM LA due to uncoupling activity and was fully inhibited by the addition of 2 mM GTP. Regarding the higher initial respiration rate in the absence of PN, we assumed that endogenous NEFA content in isolated mitochondria remained high. Interestingly, this NEFA-induced UCP1 activity was detectable even at the highest BSA concentration (1 %) used in depletion buffers during mitochondrial preparations and was fully inhibited by the addition of GTP. Moreover, final addition of 0.1 % BSA in the absence of GTP led to the same respiration rate similar to the condition where GTP inhibited the uncoupling activity. This emphasized that no artifactual uncoupling was

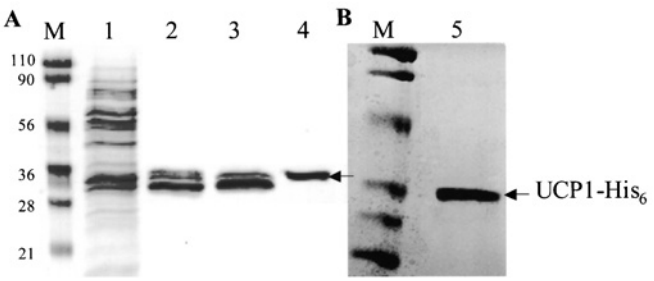

Figure 2 TX100 and DDM purification procedure of UCP1–His_6 from 40 mg of total mitochondrial proteins

(**A**) Proteins isolated from successive purification steps were subjected to SDS/PAGE (10 % gel) and analysed by Coomassie Blue staining: TX100-solubilized supernatant (10 μg, lane 1); HTP flow-through (5 μg, lane 2); supernatant after 2 h of incubation with Ni-NTA resin (5 μg, lane 3); and pure TX100-eluted fraction after treatment of the Ni-NTA resin with buffer containing 500 mM imidazole (5 μg, lane 4). (**B**) The same procedure was applied to UCP1–His_6 with exchange of 0.05 % DDM during IMAC washing step (5 μg, lane 5). Lane M, molecular mass markers (kDa).

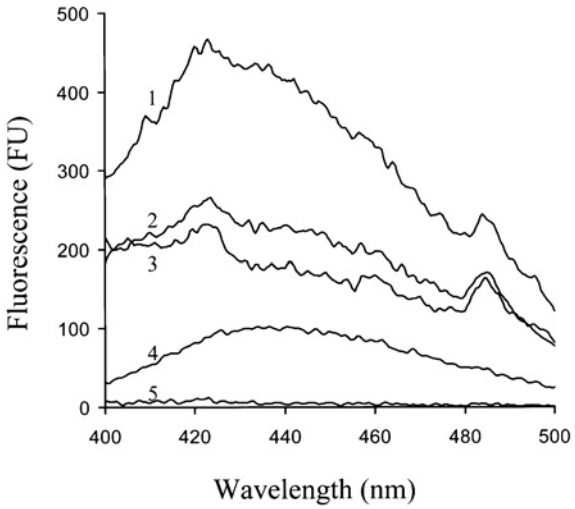

Figure 3 FRET experiments showing Mant-modified ATP binding to UCP1–His_6 and competition with unmodified nucleotide

Maximum Mant-ATP fluorescence peak was at approx. 435 nm. Fluorescence emission spectra ($\lambda_{ex} = 280$ nm) were recorded in (5) 10 mM Tris, 100 mM NaCl (pH 6.8) and 0.05 % DDM containing (1) 5 μM UCP1–His_6 and 10 μM Mant-ATP, (2) 5 μM UCP1–His_6, 10 μM Mant-ATP and 1 mM ATP, (3) 5 μM UCP1–His_6 and (4) 10 μM Mant-ATP. FU, fluorescence units.

detected during non-phosphorylating respiration experiments. Stuart et al. [12] expressed similar amounts of UCP1 in yeast using a stronger promoter, the phosphoglycerate kinase promoter (pKV49 vector), but without fusion of *UCP1* gene to a Kozak sequence that favours translation in eukaryotic cells. Under this expression condition, they demonstrated an NEFA-induced PN-insensitive uncoupling and assigned this artifactual proton leak as a function of the rate of UCP1 synthesis. However, in the present study, no significant artifactual GTP-insensitive LA-stimulated respiration was detected when GTP was present to inhibit UCP1. This might be explained by our specific conditions of expression, i.e. a mild promoter together with an upstream Kozak sequence instead of a stronger promoter in the absence of a translation enhancer.

UCP1–His_6 uncoupling activity measured on isolated mitochondria allowed us to assess whether the His epitope interfered with the UCP1 function and thus affected the native structure. Measurements of non-phosphorylating respiration clearly demonstrated that UCP1–His_6 is sensitive to one NEFA activator (LA) and one of its inhibitors (GTP).

Purification of UCP1–His_6 and nucleotide-binding measurement

UCP1 was purified earlier using solubilization and HTP steps in the presence of TX100 detergent. This procedure led to a partially pure protein suitable for subsequent functional characterizations and reconstitution experiments [24,25]. Nevertheless, we had to ensure exclusion of co-purification of any other mitochondrial proteins to envisage further biophysical analyses. Accordingly, we first developed a simple and reliable purification procedure for recombinant UCP1 expressed in yeast mitochondria. We used a nickel-chelating affinity-chromatography step, which significantly eased and accelerated purification of the recombinant His-tagged UCP1 to homogeneity.

A three-step procedure was used, which included the conventional procedure (solubilization and HTP chromatography, [24]) for isolation of UCP followed by an IMAC step (Figure 2A). When applied to the HTP column, the TX100-solubilized UCP1 was first collected in the flow-through together with two major contaminants. Solubilization conditions of mitochondria that gave maximal yield of UCP1–His_6 in the HTP supernatant were with a protein/detergent (w/w) ratio of 2. Then the IMAC batch procedure allowed us to achieve high-grade purification of the UCP1–His_6 isolated from the HTP. After 2 h of batch incubation with the resin and extensive washing in the presence of 20 mM imidazole, maximal recovering yields were obtained with two repeated treatments (1 vol. of resin each) of buffer containing 500 mM imidazole. Moreover, UCP1–His_6 was typically eluted at a final protein concentration range of 0.2–0.4 mg/ml. It is noteworthy that 20 mM imidazole allowed removal of the major contaminants but did not unbind the tagged protein, which demonstrated an efficient affinity of UCP1–His_6 for the Ni-NTA resin in contrast with the reported purification procedure of His-tagged AAC expressed in yeast [26]. Highly purified UCP1–His_6 (0.25 ± 0.06 mg; S.D. calculated on the basis of five independent preparations) was recovered from 40 mg of starting mitochondrial material. As for the estimated expression level, we assumed that approx. 40 % of UCP1–His_6 was lost during the purification procedure. Since no other proteins were detected on Coomassie Blue-stained gel, the purity was estimated to be more than 95 %. Western-blot analysis verified that no proteolysis products or oligomers were detected (results not shown).

To characterize UCP1 with spectroscopic tools, the detergent was changed because of the strong absorption interference at low wavelengths, attributable to the TX100 molecule. Accordingly, TX100 was exchanged with DDM during IMAC washing steps. DDM is a non-ionic detergent with low critical micellar concentration, close to the critical micellar concentration of TX100, and is frequently used in membrane protein crystallography. Using our purification conditions, we were able to isolate the DDM-exchanged UCP1–His_6 at approx. 60 % recovery yield and $\geqslant 95$ % purity level as shown in Figure 2(B). It is noteworthy that the purification and recovery yields were independent of the detergent.

Since UCP1 binds fluorescent nucleotides [27], commercially available Mant-modified ATP was used to determine whether our purification method affected the PN-binding conformation. As described previously for UCP2 [28], FRET experiments requiring energy transfer from the protein to the Mant-modified nucleotide showed a probe-specific fluorescence enhancement in the presence of UCP1–His_6. As shown in Figure 3, addition of 10 μM Mant-ATP to 5 μM of purified UCP1–His_6 increased approx. 2.5-fold the intensity of emission peak at 435 nm

($\lambda_{ex} = 280$ nm) due to energy transfer from the protein to the probe. Moreover, increase in the fluorescence could be displaced by competition with 1 mM unmodified ATP. The intrinsic fluorescence of 10 μM Mant-ATP in this wavelength range explained why the emission signal at 435 nm did not fully return to its initial value in the presence of the competitor and UCP1–His_6.

These results indicate that the PN-binding conformation is properly conserved after the IMAC step. Given that FRET measurements have been performed with DDM-exchanged UCP1, we also consider DDM to be suitable for further biophysical characterization.

Secondary structure of UCP1–His_6 by far-UV CD

CD spectroscopy was accordingly used to determine the secondary structure of the DDM-purified UCP1–His_6 as well as the possible conformational changes induced by the addition of an inhibitor such as GTP. Indeed, CD analysis is known to be very reliable when determining the α-helix content [29], the suspected major component of UCP (and other MCF members) secondary structures. To estimate the secondary structure from CD spectra, we assumed that analyses of CD spectra of the membrane protein by comparison with a CD spectrum reference set of well-solved structures of globular proteins produced accurate results. This point is still under debate, mainly because of peak magnitude variations due to the nature of the protein environment [30]. This is particularly true for hydrophobic proteins embedded in large membrane particles, where absorption flattening and differential scattering artifacts were observed [31,32]. In any case, differences between helix contents estimated from the structure and from the CD spectrum appear to be rather low for a number of membrane proteins, including lactose permease (80 % estimated [33] versus 78 % calculated from the structure [34]) or nicotinic acetylcholine receptor (23 % estimated [35] versus 25.5 % calculated [36,37]). At least for a largely helical protein, α-helical elements seem to produce a signal that is less sensitive to environment and finally yields correct predictions, irrespective of the wavelength range scanned during the measurement [29].

The recorded CD spectra of free and GTP-loaded UCP1–His_6 are shown in Figure 4. A qualitative analysis indicated that the spectra were dominated by the contribution of α-helices, with prominent negative bands of similar magnitudes at 222 and 208 nm and a strong positive maximum centred at 194 nm. Furthermore, comparison of the spectra obtained in the presence or absence of GTP suggested that uninhibited and inhibited UCP1 conformations did not significantly differ at the level of their secondary-structure content.

To estimate the secondary-structure content, deconvolution of free and PN-loaded UCP1–His_6 CD spectra was subsequently performed on the basis of reference CD data set. The latter contained CD spectra of 43 globular proteins of solved structure, representative of α-helix, β-sheet, β-turn and unordered elements [21]. Later, SVD calculations converged to a final solution with or without the inhibitor. Linear combination of defined CD spectra fitted suitably to the experimental CD measurements over the entire wavelength range (190–240 nm). In fact, very good normalized RMSDs, goodness-of-fit standard parameters issued from the comparison between experimental and back-calculated data [38], were obtained with the CDSSTR algorithm and reflected the accurate analysis of secondary structure (normalized RMSD < 0.005 with or without GTP). It is noteworthy that both SELCON3 and CDSSTR algorithms converged to a high helical degree (up to 70 %), but SELCON3 results were rejected due to poorer normalized RMSD values (> 0.1). Since compositions of β-sheets, β-turns and random coils can only be estimated from

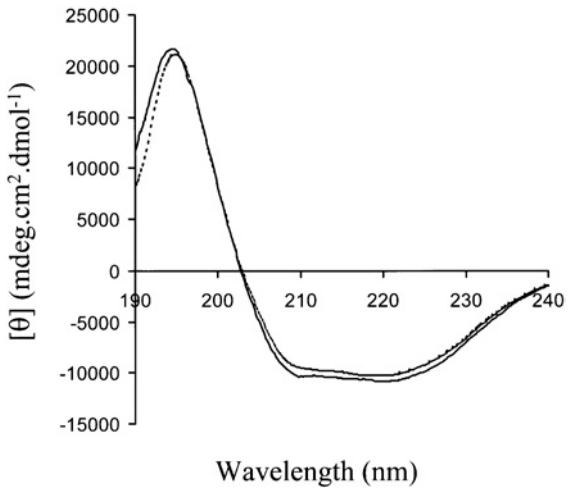

Figure 4 CD spectroscopy of highly purified UCP1–His_6

CD spectra of highly purified (5 μM) UCP1–His_6 were taken at room temperature in a 0.1-cm path length cell in 5 mM Tris and 0.3 % DDM (pH 6.8) in the absence (—) or presence (-----) of 100 μM GTP. GTP-binding equilibrium was allowed for 5 min before CD recording. Ten scans were collected for each sample at 0.2 nm intervals from 240 to 190 nm, then averaged and baseline-corrected by subtraction of blank buffer. CDSSTR-calculated helical contents estimated from CD spectra were 68 and 69 % respectively in the absence and presence of GTP.

experimental data measured to 184 nm or below [29], estimation of non-helical components was not considered as a reliable result in regard to the wavelength range of our CD spectra.

We observed that UCP1–His_6 consists of 68 % of α-helix in its free form and 69 % in its GTP-loaded conformation. These results provide the first qualitative and quantitative structural characterization of a purified UCP subfamily member. These measurements strongly suggest that the α-helix represents its predominant structural component with approx. 70 % of helical degree, which is at least 25 % higher than previous topological predictions (see the Introduction section). This high helical percentage is consistent with a model that includes six membrane-spanning α-helices and three hydrophilic α-helices within the matricial loop protrusions (see below). Furthermore, the binding of GTP does not influence the helical content since CD spectra were not significantly affected by the addition of the inhibitor.

Comparative analysis of UCP1 versus AAC1

Recently, the structure of the bovine heart AAC1 has been determined in the carboxyatractyloside-inhibited conformation to a 2.2 Å resolution [9]. The overall architecture can be described as a barrel of six transmembrane α-helices, which delimits a conical pit widely opened towards the cytosolic side. The odd-numbered helices exhibit an average length of 32 residues with a proline that induces a hinge at 2/3 from the N-terminus of the helix and cranks its C-terminal end towards the inside of the pit. The proline is located in the PX(D/E)XX(K/R) signature sequence [39], which is strictly conserved among all mitochondrial carriers and defines a hinge certainly involved in the translocation of substrates. The even helices are more hydrophilic and are approx. 25 residues long. Parallel to the matricial membrane surface, three hydrophilic 11-residue-long α-helices connecting odd- and even-numbered helices strengthen the carboxyatractyloside-inhibited conformation of the carrier. In the carboxyatractyloside-inhibited conformation, these helically shaped elements increase the helical degree to 66 %, in contrast

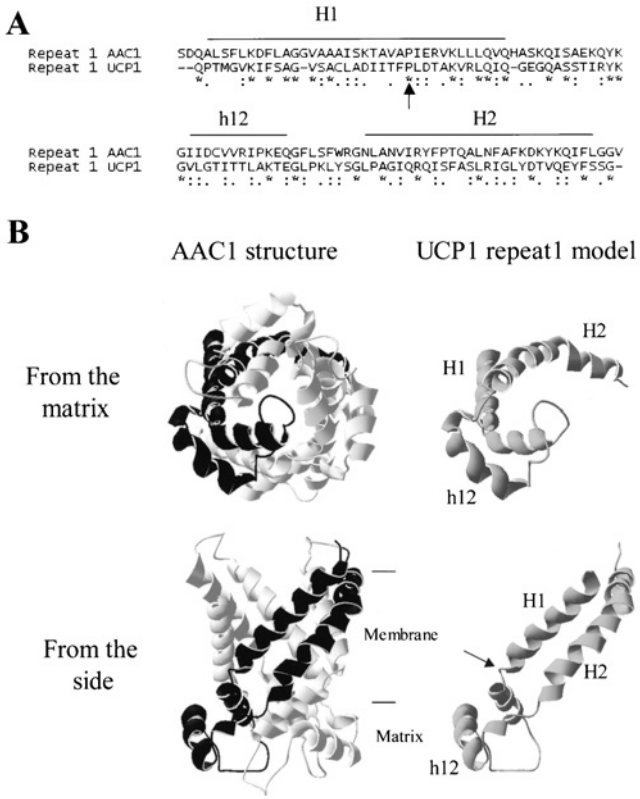

Figure 5 UCP1 repeat 1 model based on AAC1 structure

(**A**) Alignment between AAC1 repeat 1 and UCP1 repeat 1 was performed using ClustalW. Helices were located on the primary sequence. (**B**) The model was obtained by automated homology modelling (Swiss-Model) using AAC1 structure (1OKC, [7]) as the template. Same as in (**A**); H1 and H2 are the two membrane-spanning helices of the first repeat and are connected by an h12 hydrophilic helix located in the matricial loop. The position of the proline hinge is shown by an arrow. AAC1 structure is shown in light grey including repeat 1 in black. UCP1 repeat 1 model is shown in dark grey.

with previous computational predictions (< 40 %). Similarly, our CD results demonstrate a helical degree of approx. 70 % for solubilized UCP1–His_6, which is consistent with the determined α-helix content of the AAC1.

We generated the comparative model of UCP1 using the AAC1 structure as the template. Comparative modelling or homology modelling is a computational procedure by which a three-dimensional model of a target protein, in fact a target primary sequence, is built on the basis of the structure of an X-ray-resolved homologue protein. As shown in Figure 5, only the repeat 1 sequence of UCP1 was modelled for two reasons: (i) only repeat 1 of UCP1 is suitably aligned on repeat 1 of the AAC1 with 27 % homology and only two gaps; and (ii) since UCP1 has no carboxyatractyloside-inhibited conformation, we could not produce a realistic model of the entire structure of UCP1 on the basis of AAC1. With regard to the homology between repeat 1 sequences of UCP1 and AAC1, Swiss-Model was able to produce a model of the UCP1 first domain that fitted suitably on AAC1 repeat 1 (α-carbon RMSD of 0.17 Å). The overall structural fold contained three helices, i.e. two transmembrane helices H1 (N-terminus) and H2 (C-terminus) connected by a loop that included a small helix (h12) parallel to the membrane surface. The hinged H1 described for odd-numbered helices in AAC1 was also observed in UCP1 at the conserved proline level. Therefore we deduced the secondary-structure content from the obtained model: UCP1 repeat 1 model exhibited 68 % of helically shaped elements. Thus according to internal sequence homology of the repeats of UCP1 and AAC1, this estimation agrees with our CD quantification.

Conclusions

To summarize, we found quantitative evidence that α-helix is the major component of UCP1 secondary structure. Moreover, the PN-binding mechanism does not involve defined secondary-structure rearrangement as reflected by the helical content conservation in free and GTP-loaded UCP1 conformations. For secondary structure (experimental and computational data) and proline signature sequence conservation, we hypothesize that the UCP1 structure is very similar to the AAC. Long, cranked odd-numbered helices including proline hinges as well as membrane-parallel hydrophilic helices could be common features of both AAC and UCP.

This work was supported by grants from the Fonds National de la Recherche Scientifique (FRFC 2.4532.03) and from Fonds spéciaux ULg. P. D. and R. N. are recipients of the Fonds pour la Recherche Industrielle et Agronomique fellowship. A. M. is supported partially by a grant from the Fonds de la Recherche Fondamentale et Collective (contract number 2.4545.01). This work was also supported by the Belgian Government in the framework of the Pôles d'Attraction Interuniversitaires (PAI P5/33). We thank Dr L. Whitmore (University of London, U.K.) and Dr M. Galleni (University of Liege, Belgium) for their valuable advice on CD analyses and protein purification respectively.

REFERENCES

1 Walker, J. E. (1992) The mitochondrial transporter family. Curr. Opin. Struct. Biol. **2**, 519–526
2 Klingenberg, M. and Echtay, K. S. (2001) Uncoupling proteins: the issues from a biochemist point of view. Biochim. Biophys. Acta **1504**, 128–143
3 Echtay, K. S., Winkler, E. and Klingenberg, M. (2000) Coenzyme Q is an obligatory cofactor for uncoupling protein function. Nature (London) **408**, 609–613
4 Runswick, M. J., Powell, S. J., Nyren, P. and Walker, J. E. (1987) Sequence of the bovine mitochondrial phosphate carrier protein: structural relationship to ADP/ATP translocase and the brown fat mitochondria uncoupling protein. EMBO J. **6**, 1367–1373
5 Walker, J. E. and Runswick, M. J. (1993) The mitochondrial transport protein superfamily. J. Bioenerg. Biomembr. **25**, 435–446
6 Miroux, B., Frossard, V., Raimbault, S., Ricquier, D. and Bouillaud, F. (1993) The topology of the brown adipose tissue mitochondrial uncoupling protein determined with antibodies against its antigenic sites revealed by a library of fusion proteins. EMBO J. **12**, 3739–3745
7 El Moualij, B., Duyckaerts, C., Lamotte-Brasseur, J. and Sluse, F. E. (1997) Phylogenetic classification of the mitochondrial carrier family of *Saccharomyces cerevisiae*. Yeast **13**, 573–581
8 Klingenberg, M. (1990) Mechanism and evolution of the uncoupling protein of brown adipose tissue. Trends Biochem. Sci. **15**, 108–112
9 Pebay-Peyroula, E., Dahout-Gonzalez, C., Kahn, R., Trezeguet, V., Lauquin, G. J. and Brandolin, G. (2003) Structure of mitochondrial ADP/ATP carrier in complex with carboxyatractyloside. Nature (London) **426**, 39–44
10 Murdza-Inglis, D. L., Patel, H. V., Freeman, K. B., Jezek, P., Orosz, D. E. and Garlid, K. D. (1991) Functional reconstitution of rat uncoupling protein following its high level expression in yeast. J. Biol. Chem. **266**, 11871–11875
11 Bathgate, B., Freebairn, E. M., Greenland, A. J. and Reid, G. A. (1992) Functional expression of the rat brown adipose tissue uncoupling protein in *Saccharomyces cerevisiae*. Mol. Microbiol. **6**, 363–370
12 Stuart, J. A., Harper, J. A., Brindle, K. M., Jekabsons, M. B. and Brand, M. D. (2001) A mitochondrial uncoupling artifact can be caused by expression of uncoupling protein 1 in yeast. Biochem. J. **356**, 779–789
13 Kozak, M. (1986) Point mutations define a sequence flanking the AUG initiator codon that modulates translation by eukaryotic ribosomes. Cell (Cambridge, Mass.) **44**, 283–292
14 Daum, G., Bohni, P. C. and Schatz, G. (1982) Import of proteins into mitochondria. Cytochrome b2 and cytochrome *c* peroxidase are located in the intermembrane space of yeast mitochondria. J. Biol. Chem. **257**, 13028–13033
15 Lobley, A. and Wallace, B. A. (2001) DICHROWEB: a website for the analysis of protein secondary structure from circular dichroism spectra. Biophys. J. **80**, 373a
16 Lobley, A., Whitmore, L. and Wallace, B. A. (2002) DICHROWEB: an interactive website for the analysis of protein secondary structure from circular dichroism spectra. Bioinformatics **18**, 211–212

17 Compton, L. A. and Johnson, Jr, W. C. (1986) Analysis of protein circular dichroism spectra for secondary structure using a simple matrix multiplication. Anal. Biochem. **155**, 155–167
18 Manavalan, P. and Johnson, Jr, W. C. (1986) Variable selection method improves the prediction of protein secondary structure from circular dichroism spectra. Anal. Biochem. **167**, 76–85
19 Sreerema, N. and Woody, R. W. (1993) A self-consistent method for the analysis of protein secondary structure from circular dichroism. Anal. Biochem. **209**, 32–44
20 Sreerema, N., Venyaminov, S. Y. and Woody, R. W. (1999) Estimation of the number of helical and strand segments in proteins using CD spectroscopy. Protein Sci. **8**, 370–380
21 Sreerama, N. and Woody, R. W. (2000) Estimation of protein secondary structure from CD spectra: comparison of CONTIN, SELCON and CDSSTR methods with an expanded reference set. Anal. Biochem. **287**, 252–260
22 Guex, N. and Peitsch, M. C. (1997) SWISS-MODEL and the Swiss-Pdb Viewer: an environment for comparative protein modelling. Electrophoresis **18**, 2714–2723
23 Laskowski, R. A., MacArthur, M. W., Moss, D. S. and Thornton, J. M. (1993) PROCHECK – a program to check the stereochemical quality of protein structures. J. Appl. Crystallogr. **26**, 283–291
24 Lin, C. S. and Klingenberg, M. (1980) Isolation of the uncoupling protein from brown adipose tissue mitochondria. FEBS Lett. **113**, 299–303
25 Lin, C. S. and Klingenberg, M. (1982) Characteristics of the isolated purine nucleotide binding protein from brown fat mitochondria. Biochemistry **21**, 2950–2956
26 Fiore, C., Trezeguet, V., Roux, P., Le Saux, A., Noel, F., Schwimmer, C., Arlot, D., Dianoux, A. C., Lauquin, G. J. and Brandolin, G. (2000) Purification of histidine-tagged mitochondrial ADP/ATP carrier: influence of the conformational states of the C-terminal region. Protein Expr. Purif. **19**, 57–65
27 Huang, S. G. and Klingenberg, M. (1995) Fluorescent nucleotide derivatives as specific probes for the uncoupling protein: thermodynamics and kinetics of binding and the control by pH. Biochemistry **34**, 349–360
28 Jekabsons, M. B., Echtay, K. S. and Brand, M. D. (2002) Nucleotide binding to human uncoupling protein-2 refolded from bacterial inclusion bodies. Biochem. J. **366**, 565–571
29 Johnson, Jr, W. C. (1990) Protein secondary structure and circular dichroism: a practical guide. Proteins **7**, 205–214
30 Wallace, B. A., Lees, J. G., Orry, A. J., Lobley, A. and Janes, R. W. (2003) Analyses of circular dichroism spectra of membrane proteins. Protein Sci. **12**, 875–884
31 Wallace, B. A. and Mao, D. (1984) Circular dichroism analyses of membrane proteins: an examination of differential light scattering and absorption flattening effects in large membrane vesicles and membrane sheets. Anal. Biochem. **142**, 317–328
32 Wallace, B. A. and Teeters, C. L. (1987) Differential absorption flattening optical effects are significant in the circular dichroism spectra of large membrane fragments. Biochemistry **26**, 65–70
33 Kaback, H. R., Frillingos, S., Jung, H., Jung, K., Prive, G. G., Ujwal, M. L., Weitzman, C., Wu, J. and Zen, K. (1994) The lactose permease meets Frankenstein. J. Exp. Biol. **196**, 183–195
34 Abramson, J., Smirnova, I., Kasho, V., Verner, G., Kaback, H. R. and Iwata, S. (2003) Structure and mechanism of the lactose permease of *Escherichia coli*. Science **301**, 610–615
35 Mielke, D. L. and Wallace, B. A. (1988) Secondary structural analyses of the nicotinic acetylcholine receptor as a test of molecular models. J. Biol. Chem. **263**, 3177–3182
36 Brejc, K., van Dijk, W. J., Klaassen, R. V., Schuurmans, M., van der Oost, J., Smit, A. B. and Sixma, T. K. (2001) Crystal structure of an ACh-binding protein reveals the ligand-binding domain of nicotinic receptors. Nature (London) **411**, 269–276
37 Miyazawa, A., Fujiyoshi, Y. and Unwin, N. (2003) Structure and gating mechanism of the acetylcholine receptor pore. Nature (London) **423**, 949–955
38 Mao, D., Wachter, E. and Wallace, B. A. (1982) Folding of the H^+-ATPase proteolipid in phospholipid vesicles. Biochemistry **21**, 4960–4968
39 Nelson, D. R., Felix, C. M. and Swanson, J. M. (1998) Highly conserved charge-pair network in the mitochondrial carrier family. J. Mol. Biol. **277**, 285–308

Received 19 December 2003/5 February 2004; accepted 6 February 2004
Published as BJ Immediate Publication 6 February 2004, DOI 10.1042/BJ20031957